

Signal Detection and Estimation of Directional Parameters for Multiple Arrays

Approved for public release; distribution is unlimited.

August 2001



Prepared for:
Defense Threat Reduction Agency
8725 John J. Kingman Road, MS 6201
Fort Belvoir, VA 22060-6201

DSWA01-97-C-0150

Robert H. Shumway
Sung-Eun Kim

Prepared by: University of California, Davis
Department of Statistics
1 Shields Avenue
Davis, CA 95616

20020426 158

Technical Report

DESTRUCTION NOTICE:

Destroy this report when it is no longer needed.
Do not return to sender.

PLEASE NOTIFY THE DEFENSE THREAT REDUCTION
AGENCY, ATTN: ADM, 8725 JOHN J. KINGMAN ROAD,
MS-6201, ALEXANDRIA, VA 22060-6201, IF YOUR
ADDRESS IS INCORRECT, IF YOU WISH IT DELETED
FROM THE DISTRIBUTION LIST, OR IF THE ADDRESSEE
IS NO LONGER EMPLOYED BY YOUR ORGANIZATION.

REPORT DOCUMENTATION PAGE			Form Approved OMB No. 0704-0188	
Public reporting burden for this collection of information is estimated to average 1 hour per response, including the time for reviewing instructions, searching existing data sources, gathering and maintaining the data needed, and completing and reviewing the collection of information. Send comments regarding this burden estimate or any other aspect of this collection of information, including suggestions for reducing this burden, to Washington Headquarters Services, Directorate for Information Operations and Reports, 1215 Jefferson Davis Highway, Suite 1204, Arlington, VA 22202-4302, and to the Office of Management and Budget, Paperwork Reduction Project (0704-0188), Washington, DC 20503.				
1. AGENCY USE ONLY (Leave blank)		2. REPORT DATE 010800		3. REPORT TYPE AND DATES COVERED Technical 970930-990930
4. TITLE AND SUBTITLE Signal Detection and Estimation of Directional Parameters for Multiple Arrays			5. FUNDING NUMBERS C - DSWA 01-97-C-0150 PE - RDT&E PR - CD TA - CD WU - 653630	
6. AUTHOR(S) Robert H. Shumway and Sung-Eun Kim				
7. PERFORMING ORGANIZATION NAME(S) AND ADDRESS(ES) University of California, Davis Department of Statistics 1 Shields Avenue Davis, CA 95616			8. PERFORMING ORGANIZATION REPORT NUMBER Report 380	
9. SPONSORING/MONITORING AGENCY NAME(S) AND ADDRESS(ES) Defense Threat Reduction Agency 8725 John J. Kingman Road Fort Belvoir, VA 22060-6201 TDCN/Dainty			10. SPONSORING/MONITORING AGENCY REPORT NUMBER DTRA-TR-99-50	
11. SUPPLEMENTARY NOTES This work was sponsored by the Defense Threat Reduction Agency under RDT&E RMC code B 4699 C CD CD 65363 5P50 A 25904D.				
12a. DISTRIBUTION AVAILABILITY STATEMENT Approved for public release: distribution unlimited			12b. DISTRIBUTION CODE	
13. ABSTRACT (Maximum 200 words) We develop an integrated approach to estimating velocities and azimuths from a collection of local arrays and then fusing the data into Bayesian locations and their associated uncertainty ellipses. A small-array theory is developed that characterizes the performance of local optimal detectors under signal correlation and decorrelation scenarios. We compare the performance of maximum likelihood estimators such as the beam power and the generalized beam power as a function of array geometry and signal to noise ratio. Optimal local-array geometries are suggested that are relevant to the problem of designing an optimal infrasound array. Wave-number estimators along with estimated variance covariance matrices are used as input to study the size and orientation of 90% posterior probability ellipses for various likely subsets of detecting stations within the global infrasound array proposed for the Prototype International Data Center (PIDC). Adding detecting stations decreased the size of the 90% ellipse by about 10-20% per added station, whereas increasing the signal to noise ratio from 2 to 3 decreased the size of the ellipse by 30-40%. Adding an inner triangle to the conventional 1 km triangular array gave more modest reductions of 7-10%.				
14. SUBJECT TERMS Detection Infra-sound Maximum Likelihood Location Multiple Arrays			15. NUMBER OF PAGES 36	
			16. PRICE CODE	
17. SECURITY CLASSIFICATION OF REPORT UNCLASSIFIED	18. SECURITY CLASSIFICATION OF THIS PAGE UNCLASSIFIED	19. SECURITY CLASSIFICATION OF ABSTRACT UNCLASSIFIED	20. LIMITATION OF ABSTRACT SAR	

Table of Contents

Section	Page
1 Introduction	1
2 Local-Array Detection and Estimation	4
2.1 Estimation of Wave-Number Parameters	5
2.2 Theoretical Performance of Single Arrays	8
2.3 Estimation of Signal and Noise Parameters	10
2.4 Signal Detection	12
2.5 Empirical Results	13
3 Global Location Capabilities	16
3.1 Fusion Locations Via Classical and Bayesian Methods	17
3.2 Locations Using the IMS Array	19
4 Discussion	23
5 References	25
Distribution List	DL-1

Figures

Figure		Page
1	Small Fry series after aligning and delaying to correspond with an approximate velocity of .3 km/sec and an azimuth of 225 degrees sampled at .1 sec.	1
2	Proposed IMS infrasound arrays in the southwest quadrant and two hypothetical event locations marked by +.	2
3	Estimated large sample standard deviation of azimuth estimators as a function of baseline distance using the Mack-Flinn theoretical coherence model for decorrelation with distance with the solid lines for the weighted beamforming estimator and the dotted lines denoting simple beamforming.	9
4	Relief (left column) and contour (right column) plots of F-statistics for detecting infrasonic signal at two bandwidths; narrow band F shows peak at 227(10) degrees and velocity $c = .24(.04)$ km/sec.	14
5	Relief (left) and contour (right) plots of beam power and maximum likelihood correlated beam power detectors. Beam power shows peak at 225(7) degrees and velocity $V = .26(.03)$ km/sec., correlated detector shows peaks at 225(6) degrees and $.26(.03)$ km/sec.	15
6	Possible prior distributions for standard deviations of measured wave-number estimates.	18
7	Posterior probability (90 and 95%) ellipses for various array detection configurations assuming 7-element arrays, perfect signal correlation and $S/N = 2$.	21

Section 1

Introduction

The monitoring of a comprehensive test ban treaty (CTBT) depends rather critically on data collected from various networks of recording devices. Generally, there will be collections of small local seismic or acoustic arrays, providing as input, signals from a number of sensors recording a common event. For example, Figure 1 shows time series from a small array of microbarographic instruments that recorded a nuclear explosion, detonated about 25 km south of Christmas Island. The dimensions and configuration of the array are unknown so the pseudo data are constructed by aligning to a given velocity and azimuth assuming 1 km sides on the array. The problems of interest for this local array involve first detecting the signal and then identifying parameters or features that can be used to locate the source of the event. It would also be critical to determine whether the detected signal belongs to a benign class of events such as might be produced by earthquakes or mining explosions or whether it might possibly be an explosion of interest to the nuclear monitoring community. While the second discrimination aspect of the above problem is of great interest, it is the first question, namely the local array characteristics that influence location capability, that has been the focus of this present contract.

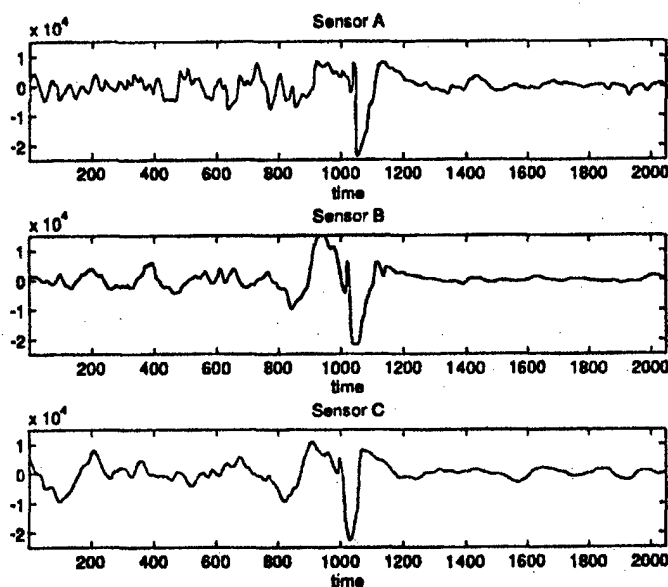


Figure 1. Small Fry series after aligning and delaying to correspond with an approximate velocity of .3 km/sec and an azimuth of 225 degrees sampled at .1 sec.

If it is supposed that a detection is available by one of the optimum processors to be consid-

ered later in this report, it will be essential to have estimators for parameters related to the location of the event. It is clear that the angle of approach or *azimuth* and the *velocity* of the signal will be related to its origin. In general, the local array provides estimators for velocity and azimuth or for two wave-numbers $\theta = (\theta_1, \theta_2)'$ that are functionally related to both the velocity and azimuth, as well as the location $x = (x_1, x_2)'$ of the event. We indicate this dependence by writing $\theta_1(x), \theta_2(x), \dots, \theta_n(x)$ for the wave-number vectors as they might be observed on n local arrays. The *global array* consists of n local arrays and the combining or *fusing* the local array estimators into an overall location estimator and its uncertainty is the objective of the analysis.

As an example of a collection of small arrays monitoring events, consider Figure 2 which shows 14 local arrays proposed for the southwest quadrant of the world-wide network of infrasound detectors to be incorporated into the International Monitoring System, denoted by IMS in the sequel. For orientation purposes, the local arrays labeled 1,2,3,4,6 and 11 are all located on the South American continent. Other stations are in the oceans to the west and east, but still south of the equator. The two hypothetical events, marked by +, are in the oceans. Location ellipses for these events developed in this report are functions of the geometry of the local array, local signal to noise ratios for the event, signal decorrelation and the time-bandwidth product. An additional important factor influencing the size of the confidence ellipses will be the configuration of detecting stations.

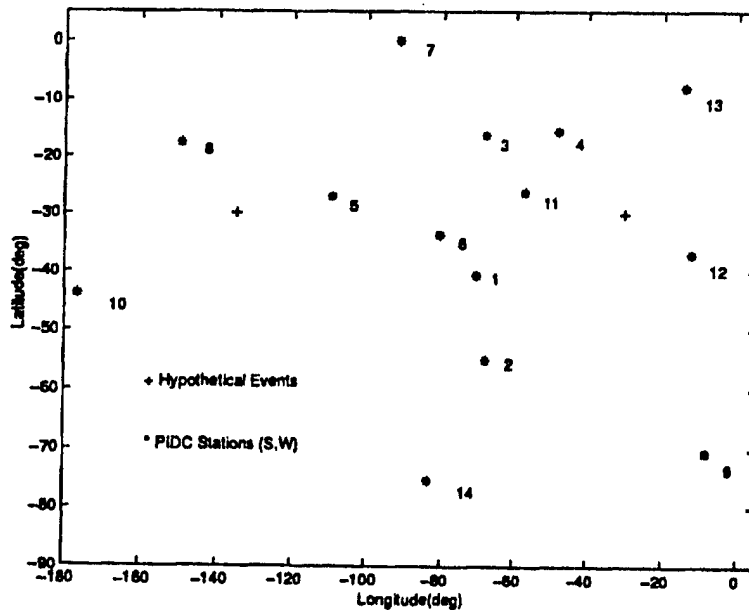


Figure 2. Proposed IMS infrasound arrays in the southwest quadrant and two hypothetical event locations marked by +.

As indicated above, the objective of this project is to develop a theory that relates the

local array performance to the location capabilities of a global network consisting of some configuration of detecting local arrays. This requires a complete investigation of local array detection and estimation using maximum likelihood; the details leading to the equations in Section 2 can be found in Shumway et al (1999).

We begin in Section 2 by estimating the wave-number parameters under the assumption that the signal and noise spectral matrices are fixed. As an adjunct to the estimation results, we obtain maximum likelihood estimators for the signal and noise spectra in the perfectly correlated case using a frequency domain version of analysis of variance. In the decorrelated signal case, we develop a version of the EM algorithm that produces separate estimators of the signal spectral matrix and the noise spectrum. This will provide estimated values for the signal coherence in the decorrelated case. As inputs for the location procedure, we also require estimated values for the wave-number parameters, say $\hat{\theta}_k$ for the $k = 1, \dots, n$ local arrays, along with their estimated variances and covariances. These estimated parameters lead to maximum likelihood estimators for velocity and azimuth. The maximum likelihood estimators for the wave-number parameters can be obtained as the maximizers of either the beam power or the F-statistic and we give the variances and covariances of these estimators under both the perfect correlation signal model and for the decorrelated signal model. Finally, we examine the variance of the estimated azimuth for various array geometries in order to evaluate the proposed triangular local arrays with various baselines.

The above results enable the development of optimal detectors for the local array that are based on frequency domain likelihood arguments, leading to statistics that are monotone functions of the usual beam power. In practice, for a perfectly correlated signal model the optimal test statistic is the ratio of the beam power to the noise power and has the F distribution. In the decorrelated signal case, which may be common when sensors in the local array are quite far apart, we obtain the likelihood ratio detector as a weighted linear combination of sample cross-spectra.

Section 3 considers optimal methods for fusing the local array wave-number vectors $\hat{\theta}_1, \dots, \hat{\theta}_n$ into an overall location and its associated uncertainty, as determined by 90 and 95% confidence or posterior probability ellipses. We consider classical nonlinear least squares methods, with ellipses determined assuming the variances are either unknown (Flinn, 1965), unknown (Everndon, 1969) or unknown with a specified prior distribution (Jordan and Sverdrup, 1981, Bratt and Bache, 1988). In particular, we evaluate the performance in locating the two events shown in Figure 2 as a function of several array geometries, signal to noise ratios and detecting configurations.

Section 2

Local Array Detection and Estimation

The local array performance can be evaluated by considering the model

$$y_j(t) = s_j[t - T_j(\theta)] + n_j(t) \quad (1)$$

for $j = 1, 2, \dots, N$ sensors recording a received signal $s_j(t)$, delayed by $T_j(\theta)$ and corrupted by an additive noise $n_j(t)$. Note that $\theta = (\theta_1, \theta_2)'$ is a vector of wave-number parameters that are nonlinearly related to velocity and azimuth and to the source location of the signal, say $\mathbf{x} = (x_1, x_2)'$. If the coordinates of the j th sensor are denoted by $\mathbf{r}_j = (r_{j1}, r_{j2})'$ and the signal is a plane wave at frequency f , measured in cycles per point, we may take

$$T_j(\theta) = -\frac{\mathbf{r}_j' \theta}{f} \quad (2)$$

as giving the relation between the time delay and the location of the j th sensor. Furthermore,

$$V = \frac{f}{\|\theta\|} \quad (3)$$

and

$$\alpha = \tan^{-1} \left(\frac{\theta_1}{\theta_2} \right) \quad (4)$$

give the relations to velocity V and azimuth α , where α is measured clockwise in radians. Generally we convert to degrees by multiplying by $180/\pi$ and interpret the angle obtained, beginning with 0 degrees north. $\|A\|^2 = \text{tr } AA^*$ will denote the usual squared norm of the matrix A , where $*$ denotes the complex conjugate transpose of the matrix.

For assumptions, we will always take the noise to be spatially white with $N \times N$ spectral matrix $P_n(f)I_N$, where I_N denotes the $N \times N$ identity matrix. The signal vector $\mathbf{s}_t = (s_1(t), \dots, s_N(t))'$ is assumed to be stationary with unknown $N \times N$ spectral matrix $\Sigma(f) = \{\sigma_{ij}(f), i, j = 1, \dots, N\}$ in the general decorrelated signal case, with squared signal coherence

$$\rho_{ij}^2(f) = \frac{|\sigma_{ij}(f)|^2}{\sigma_{ii}(f)\sigma_{jj}(f)},$$

which might possibly form the basis for a signal model. As is customary in these kinds of problems, the signal and noise are assumed to be completely uncorrelated.

A simplification of the above model is the case of perfect signal correlation, where one might as well assume the signal to be identical and random on each sensor, i.e.

$$y_j(t) = s[t - T_j(\theta)] + n_j(t), \quad (5)$$

with the added noise being uncorrelated between sensors and with identical spectrum $P_n(f)$ on each sensor. As will be seen later, this simplifies the analysis since we may now assume that the signal spectrum is $P_s(f)$ on each channel and that the signal spectral matrix is of the form $P_s(f)I_N$.

It is convenient to consider first the maximum likelihood estimation of the wave-number parameters for the two signal models (1) and (5) under the assumption that the signal and noise spectral matrices are known. Then, we move to estimating the signal and noise spectral matrices, conditionally on a fixed wave-number, by maximum likelihood. The optimum detector is based on the previous two results and the distribution theory of the F-statistic obtained allows a quantitative assessment for the significance of the detected signal.

2.1 Estimation of Wave-Number Parameters.

The estimation of the wave-number vector θ is most easily approached using the Whittle likelihood, expressed in terms of the probability approximate large sample probability distribution of the discrete Fourier transform (DFT) of the observed data, namely

$$Y_{j\ell} = T^{-1/2} \sum_{t=0}^{T-1} y_j(t) e^{-2\pi i f_\ell t}, \quad (6)$$

where $f_\ell = \ell_T/T$, $\ell = 1, \dots, L$ are a collection of frequencies in the neighborhood of some center frequency f , with ℓ_T a sequence of adjacent integers, chosen so that the collected ℓ_T/T form a band that encloses the desired center frequency. The $N \times 1$ vectors $Y_\ell = (Y_{1\ell}, \dots, Y_{N\ell})'$ are assumed to have a common multivariate complex normal distribution with zero mean and complex covariance matrix

$$\Sigma_y(f; \theta) = P_s(f) z(\theta) z(\theta)^* + P_n(f) I_N, \quad (7)$$

where

$$z(\theta) = (e^{2\pi i \tau'_1 \theta}, \dots, e^{2\pi i \tau'_N \theta})'$$

denotes the Fourier transform of the vector of delays. Details involving the maximizing the of the Whittle likelihood for the two cases below can be found in Shumway et al (1999).

CASE I: PERFECTLY CORRELATED SIGNALS

In the case of the perfectly correlated signal model (5), the spectral matrix will be of the form (7) and the log likelihood will be a monotone function of the *beam power*

$$B(\theta) = \sum_{\ell=1}^L \left| \sum_{j=1}^N Y_{j\ell} e^{-2\pi i \tau'_j \theta} \right|^2 \quad (8)$$

which is the usual observed power along a direction corresponding to the wave-number θ . Note that this is the usual beam power and is often realized by filtering the received data using a bandpass filter and then performing the beam operation in the time domain.

The main problem with using (8) directly as a signal detector is that its performance depends on the unknown signal and noise spectra, $P_s(f)$ and $P_n(f)$ under the hypothesis that a signal is present and on $P_n(f)$ when the signal is absent. We note that the approximate distribution of the test statistic is

$$B(\theta)/N \sim \left(P_n(f) + NP_s(f) \right) \frac{\chi_{2L}^2}{2L},$$

where the notation χ_m^2 denotes a chi-squared random variable with m degrees of freedom. Hence, the detection results will depend upon the number of sensors and the the unknown signal and noise parameters. The maximum likelihood estimators for these nuisance parameters are given in Section 2.2 and we note that there will be an optimal F-statistic in Section 2.3 with a distribution under noise alone that does not depend on the unknown signal and noise spectra.

In order to estimate the wave-number vector, it is conventional to plot (8) as a function of θ and to choose $\hat{\theta}$ as the maximizer of $B(\theta)$. The velocity and azimuth then follow from (3) and (4). The large-sample variances and covariances of the maximizers of (8) have been derived by Shumway et al (1999) using the Cramér-Rao lower bound. In this simple case, we obtain the large-sample covariance matrices as a function of the covariance matrix of the array coordinates

$$R = \frac{1}{N} \sum_{j=1}^N (\mathbf{r}_j - \bar{\mathbf{r}})(\mathbf{r}_j - \bar{\mathbf{r}})' \quad (9)$$

and the signal-to-noise ratio

$$r = \frac{P_s(f)}{P_n(f)}. \quad (10)$$

We have that $\hat{\theta}$ will be approximately normal with mean equal to the true mean and approximate covariance matrix

$$\text{cov}(\hat{\theta}) \approx \frac{1}{2(2\pi)^2} \frac{1}{L} \frac{1}{rN} \left(1 + \frac{1}{rN} \right) R^{-1}. \quad (11)$$

Then, defining the vectors $\theta = (\theta_1, \theta_2)'$ and $\tilde{\theta} = (\theta_2, -\theta_1)'$, we have the covariance matrix of velocity and azimuth given as

$$\text{cov} \begin{pmatrix} \hat{V} \\ \hat{\alpha} \end{pmatrix} \approx \frac{1}{2(2\pi)^2} \frac{1}{L} \frac{1}{rN} \left(1 + \frac{1}{rN} \right) \frac{1}{\|\theta\|^6} \Gamma(R^{-1}), \quad (12)$$

where

$$\Gamma(A) = \begin{pmatrix} f^2 \theta' A \theta & -f \|\theta\| \theta' A \tilde{\theta} \\ -f \|\theta\| \theta' A \tilde{\theta} & \|\theta\|^2 \tilde{\theta}' A \tilde{\theta} \end{pmatrix} \quad (13)$$

denotes a matrix function of the matrix A here and in the sequel. This exhibits nicely the dependence of the variances of azimuth and velocity on the geometry of the array, as

embodied in the covariance matrix of locations R . Note the variances also depend on the signal to noise ratio r , so that we still need an estimator for this quantity. The simplicity of the formulation in terms of the wave-number parameters is also appealing and it is the form of (11) as opposed to (12) that suggests the use of wave-number in the location procedure. In the Section 2.3, we consider estimating the signal and noise spectra using a spectral analysis of variance.

CASE II: SIGNAL DECORRELATION

Introducing signal decorrelation as a complication in the model also complicates the estimation of the wave-number and velocity and azimuth parameters. The likelihood corresponding to the general signal model (7) with signal decorrelation leads to maximizing a *generalized beam power* of the form

$$GB(\theta) = \frac{1}{P_n(f)} \sum_{j,k} \sum_{\ell} Y_{j\ell}^* Y_{k\ell} c_{jk}(f) e^{2\pi i(\tau_j - \tau_k)' \theta}, \quad (14)$$

where the weights $c_{jk}(f)$ are elements of the matrix

$$C(f) = [I_N + P_n(f) \Sigma^{-1}(f)]^{-1}, \quad (15)$$

depending specifically on the spectral matrix of the signal. We discuss a procedure for estimating this matrix in the next section. Following through the asymptotic theory for the maximizer $\hat{\theta}_G$ of $GB(\theta)$ leads to a variance covariance matrix of the form

$$\text{cov}(\hat{\theta}_G) \approx \frac{1}{(2\pi)^2} \frac{P_n(f)}{L} D^{-1}(f), \quad (16)$$

where

$$D(f) = \sum_{jk} c_{jk}(f) (\tau_j - \tau_k)(\tau_j - \tau_k)' \sigma_{kj}(f) \quad (17)$$

Again, we may convert into the covariance matrix for velocity and azimuth, obtaining

$$\text{cov} \begin{pmatrix} \hat{V}_G \\ \hat{\alpha}_G \end{pmatrix} \approx \frac{1}{(2\pi)^2} \frac{P_n(f)}{L} \frac{1}{\|\theta\|^6} \Gamma(D^{-1}), \quad (18)$$

where the matrix function $\Gamma(\cdot)$ has been defined previously in (13).

Because of the increased complexity of the maximum likelihood estimator for wave-number in the decorrelated case, it may be more useful to evaluate the classical *beam power* estimator for this case. Shumway et al (1999) show that for the estimator maximizing the beam power, say $\hat{\theta}$, it follows that

$$\text{cov}(\hat{\theta}) \approx D_1^{-1} W D_1^{-1}, \quad (19)$$

where D_1 is just D in (17), with $c_{jk} = 1$ and

$$\begin{aligned} \frac{W}{(2\pi)^2} &= \sum_{j,k,j',k'} (\mathbf{r}_j - \mathbf{r}_k)(\mathbf{r}_{j'} - \mathbf{r}_{k'})' \sigma_{jj'}(f) \sigma_{kk'}(f) \\ &+ 2P_n(f) \sum_{j,k,k'} (\mathbf{r}_j - \mathbf{r}_k)(\mathbf{r}_j - \mathbf{r}_{k'})' \sigma_{kk'}(f) + 2P_n^2(f) N^2 R. \end{aligned} \quad (20)$$

The covariance matrix of the velocity azimuth pair in this case becomes

$$\text{cov} \begin{pmatrix} \hat{V} \\ \hat{\alpha} \end{pmatrix} \approx \frac{1}{(2\pi)^2} \frac{P_n(f)}{L} \frac{1}{\|\theta\|^6} \Gamma(D_1^{-1} W D_1^{-1}). \quad (21)$$

The above results characterize the variances and covariances of the usual beam power under both the assumption that the signals are perfectly correlated and under the assumption that there is a coherence that declines, possibly as a function of distance. The next section examines these quantities as a function of array geometry at a fixed signal to noise ratio. It should be noted that the equations given in this section provide a natural set of estimated wave-numbers from each of n possible recording arrays, say $\hat{\theta}_1, \dots, \hat{\theta}_n$ and a set of estimated covariance matrices, say $\text{cov}(\hat{\theta}_1), \dots, \text{cov}(\hat{\theta}_n)$, associated with these estimated parameters. The results enable studying the problem of designing arrays as in the next section as well as the problem of fusing single array parameters into an optimal location as in Section 3.

2.2 Theoretical Performance of Single Arrays.

It is of interest to determine the array configuration that might be nearly optimal for detection and azimuth estimation of surface and underground explosions. We note that the analysis is complicated by the fact that the signal correlation will decrease as the separation between the sensors increases. Blandford (1996) has made extrapolations for coherence as a function of distance, using a model of Mack and Flinn (1971), for the distance ranges implied by an array that will have three elements arranged in a triangle with vertices separated by d kilometers and a center element. Generally speaking, coherence is reasonably high at low frequencies that are less than, say .5 Hz., but that predicted coherence goes down significantly at higher frequencies, particularly for the separation of around 1 km that predominates for the triangular array under consideration.

It is interesting to compute the azimuthal standard deviations implied by the Mack-Flinn coherence model for various intersensor separations on the simple triangular array with a center element. The approach taken here assumes that either the values maximizing the beam or the generalized beam will be used, with the variances computed from the appropriate asymptotic expressions (18) and (21) respectively. Figure 3 shows the results at various distance ranges and periods. It is clear that the beam and generalized beam behave similarly, except at the longer distance ranges. The signal to noise ratio r was taken as .75², which is regarded as sufficient for an analyst to declare a detection. Bandwidths were

.01, .02, .04 and .2 Hz respectively for cases (a)-(d) in Figure 3. Azimuthal uncertainties are larger for longer periods and actually get quite small for the higher frequencies. One second period standard deviations remain below 1 degree for intersensor distances less than one km. It is interesting to note that the minimum variance is obtained for separation distances that are exactly equal to the period, i.e. 20 km for a 20 sec period, 10 km for a 10 second period, 5 km for a 5 second period and 1 km for a 1 second period.

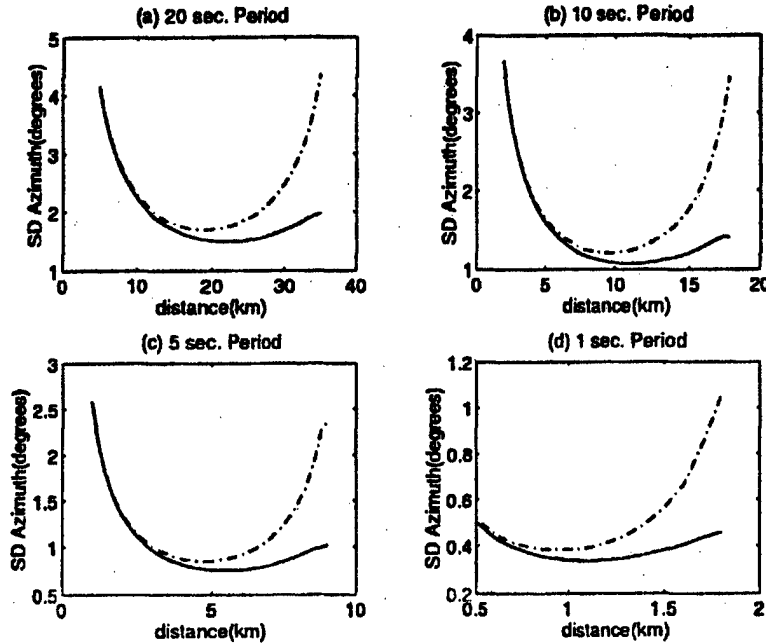


Figure 3. Estimated large sample standard deviation of azimuth estimators as a function of baseline distance using the Mack-Flinn theoretical coherence model for decorrelation with distance with the solid lines for the weighted beamforming estimator and the dotted lines denoting simple beamforming.

Blandford (1996) also increases the number of elements, considering an $N = 7$ element array consisting of the array above plus a small inverted interior triangle, with .2 km on a side. With a signal to noise ratio of $(.75)^2$, standard deviations were in the .5-2.0 degree range for periods less than 5 seconds. However, there is little improvement for 10 and 20 second periods. Blandford (1996) summarizes the computation by noting that for the 5 second period signal, which is expected from a 1 kt atmospheric nuclear explosion, the 1 kilometer array would have an azimuth estimation error approximately equal to the best historically observed residual error. The conclusions are somewhat preliminary because the underlying data is available only for much long periods and small inter-sensor distances. Analysis of additional signal data at more appropriate periods and spacings is of critical importance.

2.3 Estimation of Signal and Noise Parameters.

In the previous sections, we have regarded the signal and noise spectra, $P_s(f)$, $P_n(f)$ in the perfectly correlated case to be known. In the decorrelated case, we need to know the entire $N \times N$ spectral signal matrix $\Sigma(f)$. It turns out that maximum likelihood estimators are available for these nuisance parameters and these estimators are summarized in the following subsections.

CASE I: PERFECTLY CORRELATED SIGNALS

For the perfectly correlated case the log likelihood reduces to

$$\ln L(\theta, P_s, P_n) \propto -NL \ln P_n - L \ln(1 + rN) + \frac{B(\theta)}{P_n(N + 1/r)} \quad (22)$$

and may be maximized directly, as a function of the signal to noise ratio r and P_n . We obtain, for a fixed value of θ ,

$$\hat{P}_n(\theta) = \frac{SSE(\theta)}{(N - 1)L}, \quad (23)$$

where $SSE(\theta)$ is an error sum of squares about the fitted signal and may be written as

$$SSE(\theta) = \sum_{j=1}^N \sum_{\ell=1}^L |Y_{j\ell}|^2 - \frac{B(\theta)}{N}. \quad (24)$$

The signal spectrum is estimated by

$$\hat{P}_s(\theta) = \frac{1}{N^2 L} \left(B(\theta) - NL \hat{P}_n(\theta) \right) \quad (25)$$

We may then apply maximization alternatively, first for θ over $B(\theta)$ and then solve for $\hat{P}_s(\theta)$ and $\hat{P}_n(\theta)$ using (23) and (25). A new value of θ may be estimated by maximizing the log likelihood (22) and the obvious iterative pattern will converge by standard alternate maximization results (see Meng and Rubin, 1991). Alternatively, one may simply stop after the first step.

CASE II: SIGNAL DECORRELATION

For the multivariate signal model with signal spectral matrix $\Sigma(f)$, there are no simple estimators but we may still derive a procedure for maximizing the log likelihood using either a Newton-Raphson approach and the vector scores and information matrix or the EM algorithm on the complete data log likelihood. Now, regarding the generating model in the frequency domain as

$$Y_{j\ell} = z_j(\theta) S_{j\ell} + N_{j\ell}, \quad (26)$$

we may write the vector version as

$$Y_\ell = Z(\theta) S_\ell + N_\ell, \quad (27)$$

where $Z(\theta) = \text{diag}(z_1(\theta), \dots, z_N(\theta))$ is a diagonal and $S_t = (S_{1t}, S_{2t}, \dots, S_{Nt})'$ is the random frequency domain signal vector with spectral matrix $\Sigma(f)$. Considering the complete data, in the sense of Dempster et al (1977), as the signal vector above plus the noise vectors N_1, N_2, \dots, N_L , we obtain

$$\begin{aligned} \ln \bar{L}(\theta, \Sigma, P_n) &= -L \ln |S| - \sum_{t=1}^L S_t^* \Sigma^{-1} S_t \\ &\quad - LN \ln P_n - \frac{1}{P_n} \sum_{t=1}^L \|N_t\|^2 \end{aligned} \quad (28)$$

for the complete-data log likelihood. To maximize the original incomplete data log likelihood, we consider applying the *Expected Conditional Maximization* (ECM) algorithm of Meng and Rubin (1993). In this version of the EM algorithm, we apply the expectation and maximization steps for a given $\hat{\theta}$, where $\hat{\theta}$ is the maximizer for a fixed Σ, P_n . Note that the EM algorithm of Dempster Laird and Rubin (1977) is a rather convenient way of handling maximum likelihood estimation in multidimensional random signal context (see Shumway, 1988). Now applying the E-step of the EM algorithm to the complete data log likelihood above for a fixed θ gives

$$\hat{\Sigma} = L^{-1} \sum_t \left(\tilde{S}_t(\theta) \tilde{S}_t^*(\theta) + \tilde{\Sigma}(\theta) \right) \quad (29)$$

for the next iterate of the signal spectral matrix, where

$$\tilde{S}_t(\theta) = \left(I + P_n \Sigma^{-1} \right)^{-1} Z^*(\theta) Y_t \quad (30)$$

and

$$\tilde{\Sigma}(\theta) = P_n \left(I + P_n \Sigma^{-1} \right)^{-1}, \quad (31)$$

using results from Shumway et al (1999). The estimator for the noise spectrum will be

$$\hat{P}_n = (NL)^{-1} \sum_t \left(\|Y_t - Z(\theta) \tilde{S}_t(\theta)\|^2 + \text{tr}(Z(\theta) \tilde{\Sigma}(\theta) Z^*(\theta)) \right) \quad (32)$$

To apply the iterative ECM algorithm, one might use the following sequence of steps.

1. Determine an initial estimator for $\hat{\theta}$ as the maximizer of the beam power $B(\theta)$ as given by (8).
2. Compute initial estimators for \hat{P}_n and $\hat{\Sigma} = \hat{P}_n I$, assuming no signal correlation, using (23) and (25).
3. Update $\tilde{S}_t(\hat{\theta})$ and $\tilde{\Sigma}(\hat{\theta})$ from (30) and (31).
4. Update $\hat{\Sigma}$ and \hat{P}_n using (29) and (32).

5. Repeat steps 3. and 4. to convergence
6. Update θ by finding the maximizer of $GB(\theta)$ in (29).
7. Return to 3.

The above procedure is rather involved and it is often the case that one can estimate the signal spectral matrix from prior data, assuming that the signal spectral matrix is known in the generalized beamformed estimator $GB(\theta)$. This is illustrated in Section 2.2 where we assigned a functional form to $|\rho_{jk}|$, where $\sigma_{jk}(f) = P_s(f)|\rho_{jk}|$ based on a theoretical relation between coherence and distance.

2.4 Signal Detection.

Detecting a signal depends on developing a test statistic that does not depend on any nuisance parameters under noise alone and is a convenient function of the signal spectra under the signal hypothesis. We indicate below how to use the results of the previous section to develop the F-statistic as an optimal detector in the case of a perfectly correlated signal and give some results on the expected performance of the beam under the decorrelated signal case.

The results enable a prediction of the performance of each local array as a function of signal to noise ratio in the perfectly correlated case or as a function of the spectral matrix of the signal in the decorrelated signal case.

CASE I: PERFECTLY CORRELATED SIGNALS

Shumway et al (1999) establish that the test statistic

$$F(\hat{\theta}) = \frac{(N-1)}{N} \frac{B(\hat{\theta})}{SSE(\hat{\theta})} \quad (33)$$

has asymptotically a central F-distribution with $2L$ and $2L(N-1)$ degrees of freedom when there is no signal, where $B(\hat{\theta})$ is the beam power defined in (8) and $SSE(\hat{\theta})$ is the error power defined in (24). The F-statistic is evaluated at the estimated $\hat{\theta}$ and the approximate distribution is given by

$$F(\hat{\theta}) \sim (1 + N\tau) F_{2L, 2L(N-1)} \quad (34)$$

under the hypothesis that the signal is present, giving a computational method for establishing the false alarm rate and detection probabilities of the detector as a function of the signal to noise ratio $\tau = P_s/P_n$.

CASE II: SIGNAL DECORRELATION

In the case of a decorrelated signal, the optimal detector becomes the likelihood ratio detector, which will be a monotone function of the generalized beam $G(\hat{\theta})$. One can follow this argument through as in Shumway et al (1999) but we simply mention here that it may be

more realistic to present results involving the simple beamforming statistic, written in the form

$$B(\theta) = \sum_{\ell=1}^L |z^*(\theta) Y_{\ell}|^2$$

Now, for the general correlated signal model, we have that Y_{ℓ} have mean zero and covariance matrix

$$\Sigma_y(f) = Z(\theta)\Sigma(f)Z^*(\theta) + P_n(f)I_N. \quad (35)$$

It follows that

$$B(\theta) \sim \left(z^*(\theta)\Sigma_y(f)z(\theta) \right) \chi_{2NL}^2,$$

which simplifies, on substituting on the right hand side from (35) to

$$B(\hat{\theta}) \sim \left(\sum_{j=1}^N \sum_{k=1}^N \sigma_{jk}(f) + NP_n(f) \right) \chi_{2NL}^2, \quad (36)$$

and enables the prediction of the performance of the beam as a function of the signal spectral matrix and noise spectra. Note that we have replaced the wave-number by an estimator $\hat{\theta}$ converging to θ in probability.

2.5 Empirical Results.

We look first at a simple example involving the three sensors in Figure 1, that recorded the event Tanana at a small triangular array on Palmyra Island. To provide a baseline example, we took 2048 points (about 200 seconds) of data and re-aligned the signal to correspond to an approximate velocity of .3 km/sec and an approximate azimuth of 225 degrees. The array geometry was a triangle with 1 km sides at locations $r_1 = (0, .577)'$, $r_2 = (.5, -.289)'$ and $r_3 = (-.5, -.289)'$, leading to a diagonal covariance matrix R in (9) that has 1/6 on the diagonals. The re-aligned signals at sensors A, B and C are shown in Figure 1; the signal spectrum was centered at .044 Hz (cycles per second), i.e., at a period of about 23 sec. The coherence between sensors was reasonably high, in this case, with values .86, .83 and .82 for the three inter-sensor pairs. Hence, there is reason to believe that random univariate signal model (5) will work reasonably well.

In order for the large L asymptotics to have a chance, we first chose a band broad enough to include the entire signal, with $L=17$ frequency ordinates in the band running from .005 to .08 Hz. The estimated signal-to-noise ratio $P_s/P_n = 1/r$, in this band, using the maximum likelihood estimators (23) and (25), was 3.16. For the broad band, the estimator for the velocity was .26(.03) km/sec, using (8) and (4) to get the estimator and (12) to get the standard deviation (in parentheses). This compares to the velocity of .30 km/sec that we that input by lining up the largest minima of the signal on each sensor with this velocity. The azimuth estimator is 225(7) degrees, which is right on the known azimuth. The standard deviation implies an approximate 95% confidence interval from 211 to 239 degrees. For

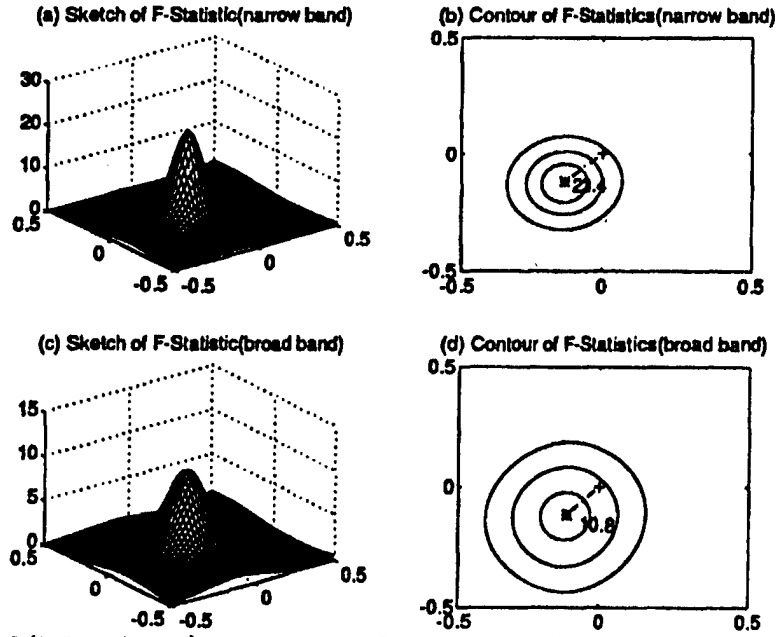


Figure 4. Relief (left column) and contour (right column) plots of F-statistics for detecting infrasonic signal at two bandwidths; narrow band F shows peak at 227(10) degrees and velocity $c = .24(.04)$ km/sec.

comparison, we tried a narrow band estimator, based on $L=3$ frequency ordinates, in the band running from approximately .040 to .048 Hz. The signal-to-noise ratio in this band was 7.36 and the estimated velocity of .24(.05) km/sec is still slightly off. Again, the azimuth estimator was 227(10) degrees with a slightly larger uncertainty. The increase in the signal-to-noise ratio in the narrower band does not completely compensate for the loss in bandwidth.

Figure 4 shows the relief plots (a) and (c) and contour plots (b) and (d) of the F-detector given by the F-statistic (41). The detector is plotted as a function of the wave number coordinates $-.5 \leq \theta_1, \theta_2 \leq .5$, where the slowest velocity in the plot corresponds to the velocity on one of the edges, e.g. $\theta_1 = \theta_2 = .5$, or .062 km/sec, using (4). Very high velocities occur near the center $\theta_1 = \theta_2 = 0$, which corresponds to an infinite velocity. The azimuth can be seen visually as the angle made by a line drawn from the center to the maximum; here, it is 225 degrees. Note that the asymptotics for this will be less sensitive to large L results, although one will still need to have the sample length T large. The plotted F-Statistic, for the narrow band case has $2L = 2(3) = 6$ and $2L(N-1) = 6(2) = 12$ degrees of freedom. Note that $F_{6,12}(.01) = 4.82$ and $F_{6,12}(.001) = 8.38$ so that the .01 and .001 significance points are exceeded by all velocities and azimuths within the first two contours of the top plot. The plotted F-Statistic, for the broad band case has $2L = 2(17) = 34$ and $2L(N-1) = 34(2) = 68$ degrees of freedom. Note that $F_{34,68}(.01) = 1.95$ and $F_{34,68}(.001) = 2.42$ so that the .01 and .001 significance points are exceeded by all velocities and azimuths within the first two

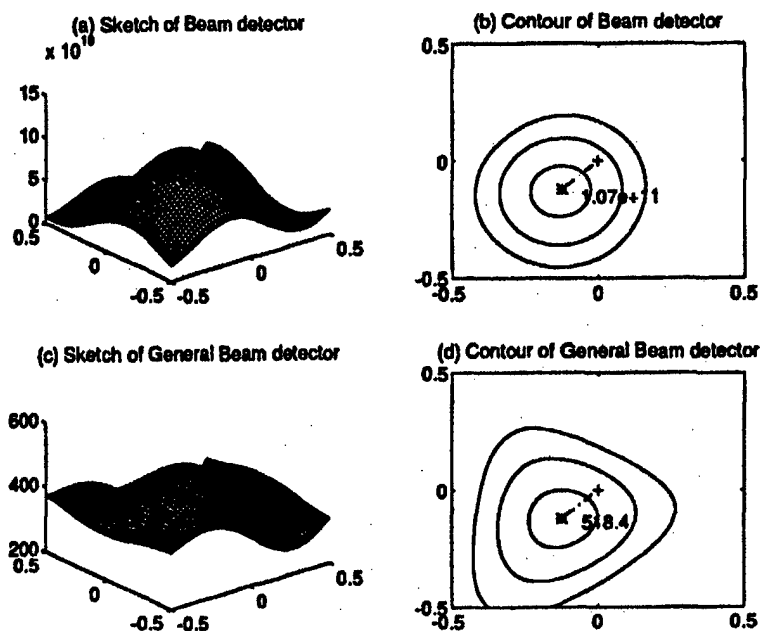


Figure 5. Relief (left) and contour (right) plots of beam power and maximum likelihood correlated beam power detectors. Beam power shows peak at 225(7) degrees and velocity $V = .26(.03)$ km/sec., correlated detector shows peaks at 225(6) degrees and $.26(.03)$ km/sec.

contours of the bottom plot.

It is also of interest to determine the estimated velocities and azimuths and their uncertainties under the coherence structure estimated at the array. This requires estimating the variance of the beamformed estimator maximizing $B(\theta)$ under the assumption that there is less than perfect coherence using (21). This can be compared to the variance of generalized beam maximizing $GB(\theta)$, given by (18). Both equations require estimating the $N \times N$ signal spectral matrix $\Sigma(f)$ and the noise spectrum $P_n(f)$. In the case of the $\hat{\theta}$ maximizing the beamforming estimator, we used (29)-(32) and the EM steps 1 to 5 to obtain the maximum likelihood estimators for $\Sigma(f)$ and $P_n(f)$, with θ fixed at $\hat{\theta}$. For the case of $\hat{\theta}_B$, the maximizer of the general beam, we simply used the ECM algorithm, following Steps 1-7 as given. Figure 5 shows the results using a slightly broader band ($L=19$) and we note that the estimators and their standard errors are nearly the same, a reflection, no doubt of the relatively high empirical coherence between the three sensors in this case.

Section 3

Global Location Capabilities

Integrating or fusing data from the single-array sources into a best overall location, with an uncertainty region provided, will be an important aspect of evaluating the predicted performance of the IMS network shown in Figure 2. Hence, we consider a methodology for using the information developed in the detection and estimation portions of this proposal for estimating the location vector $\mathbf{x} = (x_1, x_2)'$. In general, we propose a model of the form

$$\hat{\theta}_k = \theta_k(\mathbf{x}) + \mathbf{e}_k, \quad (37)$$

where $\hat{\theta}_k = (\hat{\theta}_{1k}, \hat{\theta}_{2k})'$, $k = 1, \dots, n$ are the estimated wave-number vectors, as computed from maximizing the beam power (8), or F-statistic (33) at the k^{th} array and

$$\theta_k(\mathbf{x}) = \frac{f_k}{V_k} \frac{\mathbf{x} - \mathbf{c}_k}{\|\mathbf{x} - \mathbf{c}_k\|} \quad (38)$$

gives the theoretical connection between the wave-number parameters and location. In (38), f_k is the center frequency, V_k is velocity and $\mathbf{c}_k = (c_{1k}, c_{2k})'$ denotes the coordinates of the k^{th} array. It can generally be assumed that velocity is known or can be inferred from the wave-number plot. It should be noted that there are often separate phases at the same array that may have their own estimated $\hat{\theta}_k$ and these are included under those that possibly contribute to the model (38). Under certain conditions, there may also be estimators of travel times \hat{t}_k , where $t_k(\mathbf{x}) = \|\mathbf{x} - \mathbf{c}_k\|/V_k$, perhaps from cross-correlation or other means, that could be added to the observations on location \mathbf{x} . This general framework also does not preclude the possibility of adding seismic travel times or hydroacoustic information to the stack.

A possible assumption for the bivariate error terms in (37) is that they are independent and identically distributed with mean zero and 2×2 covariance matrix

$$\text{cov } \mathbf{e}_k = \sigma^2 \Sigma(\hat{\theta}_k), \quad (39)$$

where the matrix $\Sigma(\hat{\theta}_k)$ comes from (11), specialized to the k^{th} array. Note that the components of (11) will vary according to the array size and geometry, signal-to-noise ratio and the time-bandwidth product. The scaling variance σ^2 is to account for additional variability from geophysical sources or from the observed error in a particular event location. We have used the scaling rather an additive model for the geophysical error expansion to simplify the Bayesian computation. If there are consistent biases associated with particular regions or subsets of arrays, constant correction terms can be added to the defining Equation (37). If a number of events are available, the correction terms may even be estimated by least squares using consistent source-receiver pairs.

As an example of a small demonstration set, we consider Figure 2, which shows 14 IMS array centers c_k proposed for the southwest quadrant of the world-wide network. For purposes of illustration, we also show two hypothetical events that might generate observed wave-number parameters $\hat{\theta}_k, k = 1, \dots, n$ for incorporation into the location model defined in (37) and (38). In Section 3.1, we discuss an approach to combining or fusing the wave-number parameters into an overall location, based on a given fixed set of recording arrays and their characteristics, as defined by the signal-to-noise ratio r , the time-bandwidth product BT and the array geometry, as it is expressed in terms of R and N in (11).

3.1 Fusion Locations Via Classical and Bayesian Methods.

We extend the classical methods first to the case where we observe wave-number parameters and their covariance matrix from n arrays and wish to combine or *fuse* the information into an overall location. The nonlinear model (37) and (38) can be treated in the usual way. That is, expand $\theta_k(x)$ around some initial value, say $x = x_0$ and write a linearization as

$$\hat{\theta}_k - \theta_k(x_0) = A_k(x_0)(x - x_0) + e_k, \quad (40)$$

where

$$A_k(x) = \frac{\partial \theta_k(x)}{\partial x} \quad (41)$$

is the usual 2×2 matrix of partial derivatives of $\theta_k(x)$. Then, stacking the $n, 2 \times 1$ wave-number vectors and minimizing the weighted sum of squared errors can be done by successively estimating $\beta = x - x_0$. This leads to

$$\hat{x} = \hat{x}_0 + C^{-1}(x_0) \sum_{k=1}^n A_k(x_0)' \Sigma^{-1}(\hat{\theta}_k) [\hat{\theta}_k - \theta_k(x_0)], \quad (42)$$

where

$$C(x_0) = \sum_{k=1}^n A_k(x_0)' \Sigma^{-1}(\hat{\theta}_k) A_k(x_0). \quad (43)$$

It follows that the estimated covariance matrix of the final estimator is

$$\text{cov } \hat{x} = \sigma^2 C^{-1}(\hat{x}). \quad (44)$$

Equations (42) and (43) exhibit the *fusion estimators* at each stage as pooled estimators over the n arrays as long as the variances are known. We may also develop a confidence ellipse for the fusion estimators under assumptions (A), (B) and (C), as given below.

A. VARIANCE KNOWN

We may assume that the variance σ^2 is known, either from the statistical variances of the computed wave-number estimators or from a combination of factors including the statistical

wave-number variances. In this case, the generalization of the usual chi-squared ellipse considered by Evernden (1969) can be computed from the fact that

$$(x - \hat{x})' C(\hat{x}) (x - \hat{x}) \sim \sigma^2 \chi_2^2, \quad (45)$$

where \sim denotes *is distributed as* and χ_2^2 denotes a chi-squared distribution with 2 degrees of freedom. Note that the statistical uncertainty of the wave-number estimators is already in the matrix $\Sigma(\hat{\theta}_k)$ so that a plausible estimator for σ^2 in the absence of other factors might be unity.

B. VARIANCE UNKNOWN

If variances are known only up to the constant σ^2 , this scaling variance may be estimated from the set of arrays that record the event. For the Gaussian case, the maximum likelihood estimator is proportional to the unbiased estimator

$$s^2 = \frac{1}{2(n-1)} \sum_{k=1}^n (\hat{\theta}_k - \theta_k(\hat{x}))' \Sigma^{-1}(\hat{\theta}_k) (\hat{\theta}_k - \theta_k(\hat{x})). \quad (46)$$

This case, originally considered in Flinn(1965), leads to a confidence interval based on the F-distribution, namely

$$(x - \hat{x})' C(\hat{x}) (x - \hat{x}) \sim 2s^2 F_{2,2(n-1)}, \quad (47)$$

where $F_{2,2(n-1)}$ denotes the F-distribution with 2 and $2(n-1)$ degrees of freedom.

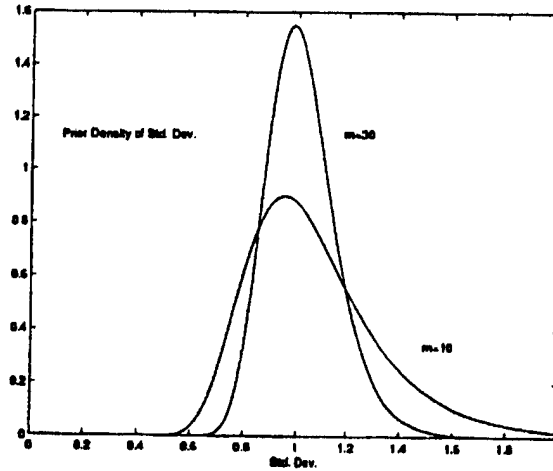


Figure 6. Possible prior distributions for standard deviations of measured wave-number estimates.

C. VARIANCE SUBJECT TO PRIOR DISTRIBUTION

It is often the case that it is unrealistic to assume that the variance is known exactly because the ellipse defined by (45) becomes too small. For a small number of arrays, the ellipse based

on the F-statistic (47) is often much too large. A useful compromise, introduced by Jordan and Sverdrup (1981) and continued by Bratt and Bache (1988), is to quantify the initial uncertainty about σ^2 by assigning it a prior distribution with density function $\pi(\sigma^2)$. It is convenient to use the inverted chi-squared distribution with parameters m , representing the equivalent sample size embodied in the prior information and σ_0^2 , representing a prior centering value for the variance. For the form of the density function, see Anderson (1984). Figure 6 plots the density function for the standard deviation σ for $\sigma_0 = 1$ and $m = 10, 30$. We note that the two values put the standard deviation between .4 and 2 for $m = 10$ and between .6 and 1.6 for $m = 30$. For a fully Bayesian approach, we assume a non-informative prior on $(-\infty < x_1, x_2 < \infty)$ for the location x and compute the posterior distribution, given the wave-number observations, as a bivariate t-distribution with 2 and $2(n-1) + m$ degrees of freedom. The posterior estimator for the variance is

$$\sigma^2 = \frac{2(n-1)s^2 + m\sigma_0^2}{2(n-1) + m}, \quad (48)$$

implying that the best approach is simply to pool the initial variance σ_0^2 and the sample variance s^2 , weighted by their degrees of freedom. The quadratic form involving the location vector x in the multivariate t has an F-distribution, making the 95% posterior probability ellipse for the location expressible as

$$(x - \hat{x})' C(\hat{x}) (x - \hat{x}) \sim 2\sigma^2 F_{2, 2(n-1)+m} \quad (49)$$

It is interesting that the form of the posterior probability ellipse (49) is similar to (47) but will be tighter because of the additional degrees of freedom for the F-statistic. Hence, the Bayesian solution represents a compromise between (45) and (47), the methods of (A) and (B).

3.2 Locations Using the IMS Array.

Given the theoretical developments of the previous sections, it is now possible to begin to assess the potential location capabilities of the reduced IMS network shown in Figure 2. It is likely that there will be relatively few stations recording each event so we will make computations based on the Bayesian approach described in (C) of the previous section. The natural measure of error in the estimated location is the confidence ellipse in the classical methods (A) and (B) and the posterior probability ellipse for the Bayesian approach described in (C).

For the small-scale example considered here, the following inputs are needed to estimate location capability. We confine this particular example to the perfectly correlated case although it is obvious that this would not be constraint because of the separate analysis available for decorrelated arrays.

SIGNAL TO NOISE RATIO

The signal to noise ratio r , defined in (10) as the ratio of the signal spectrum to the noise spectrum, is critical for determining the covariance input (11) which is needed for the covariance matrix $\Sigma(\hat{\theta}_k)$ in the posterior probability intervals. The signal to noise ratio also determines the detection probability from (34), when the signal is present; this determines the probable configuration of recording stations. The signal to noise ratio can be estimated using (23) and (25) if data are available or it can be assumed from known operating conditions. For the example given here, it is assumed to be $r = 2, 3$.

ARRAY GEOMETRY

The geometry of each local array affects the detection probability (34) and the estimated covariance of the input wave-number parameter $\Sigma(\hat{\theta}_k)$ in (11), essentially through the number of sensors, N , and the covariance matrix of the sensor locations R . In the example given next, we took two array geometries (see Blandford, 1996), namely a triangle with a 1 km baseline and a center element ($N=4$) and an extended version that adds an interior inverted inner triangle with baseline distance .2 km ($N=7$).

TIME-BANDWIDTH PRODUCT, FREQUENCY, VELOCITY

The time-bandwidth product $L = BT$ affects both the covariance matrix $\Sigma(\hat{\theta}_k)$ in (11) and the detection probability (34). Again this will change both the input covariance for the location computation and will be a determinant of the configuration of detecting local arrays. We assumed here a center frequency of 1 Hz and a time-bandwidth product of $BT = 17$, which represented a reasonable compromise from our earlier work (Shumway et al, 1999) with a Pacific Islands event. Velocity was assumed to be .3 km/sec in the example but it could be estimated for a given event at a given station using (3).

PRIOR DISTRIBUTION OF SCALING VARIANCE

As an approximate prior distribution for the scaling variance σ^2 , we can examine plots like Figure 6 for various degrees of freedom, m , which can be regarded as the equivalent sample size that would have been required to produce the required degree of accuracy for σ^2 . For purposes of illustration, assume that we expect the variance to be $\sigma_0^2 = 1$ with some spread about the value, corresponding to $m = 10$. This is probably optimistic as one might expect scaling due to geophysical causes to be somewhat greater than unity but the value 1 provides a reasonable illustrative constant. Figure 6 shows the range of values that could be expected with this choice and we assumed that the sample variance $s^2 = 1$ would have been computed using (46).

Using the above specifications gives the posterior estimators for the variance from (48) with $n = 4$ and $n = 7$ corresponding to the two local array configurations. Assuming the true location at $x = x_0$, corresponding to the two known locations marked in Figure 2 gives reasonable scenarios for event location. The posterior probability ellipses can be computed

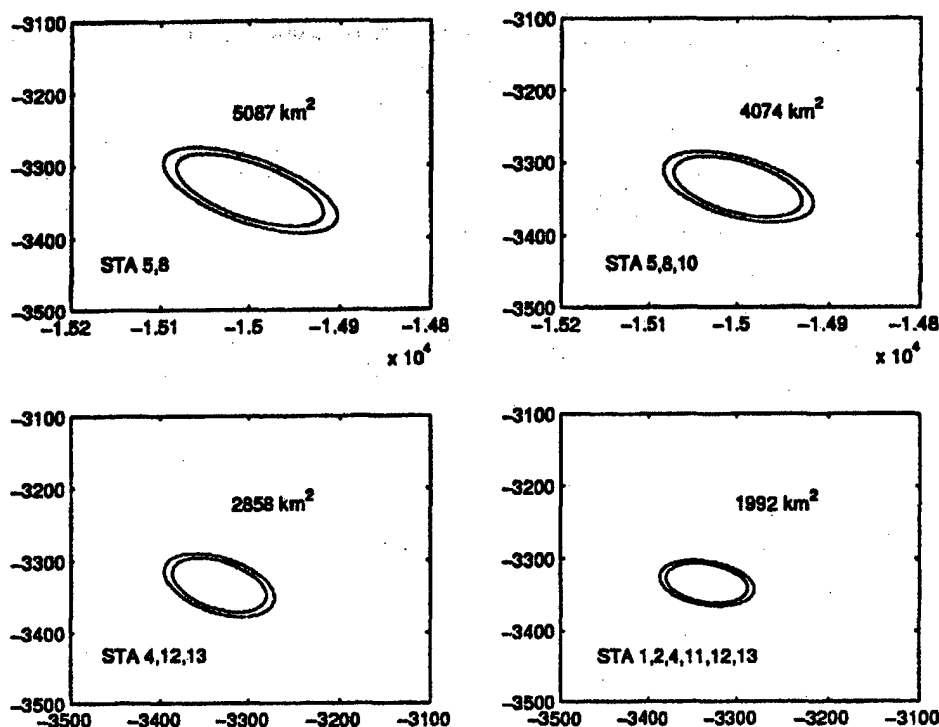


Figure 7. Posterior probability (90 and 95%) ellipses for various array detection configurations assuming 7-element arrays, perfect signal correlation and $S/N = 2$.

using (49) as a function of x , evaluated at $\hat{x} = x_0$, with $C(x_0)$ computed from (43).

Figure 7 shows the resulting posterior probability ellipses for the extended array ($n = 7$), assuming some typical recording configurations. For Event 1, we assumed two configurations of the closest three stations (5,8,10) detected the event. Note that the area of the 90% ellipse decreased by about 20% in going from two to three station detection. For Event 2, comparing $n = 4$ station detection against $n = 7$ station detection reduced the area of the ellipse by about 30%.

Table 1 gives a more detailed accounting as to what happens for various scenarios over the recording configurations in Figure 7. Here, we see 30-40% reductions achieved by increasing the signal to noise ratio from 2 to 3. Reductions achieved by adding the three center elements are more modest, on the order of 7-10%.

Table 1: Areas (km²) of 90% Posterior Probability Ellipses for Simple and Extended Triangular Arrays

	Triangular Array		Extended Array	
Stations/Event	$S/N = 2$	$S/N = 3$	$S/N = 2$	$S/N = 3$
5,8/1	5554	3566	5087	3316
5,8,10/1	4448	2856	4074	2656
4,12,13/2	3129	2002	2858	1863
1,2,4,11,12,13/2	2176	1397	1992	1299

Section 4

Discussion

In this project we have developed an integrated approach to estimating velocities and azimuths from a collection of local arrays and then fusing the data into Bayesian locations and their associated uncertainty ellipses. A small-array theory is developed that characterizes the performance of local optimal detectors under signal correlation and decorrelation scenarios. We compare the performance of maximum likelihood estimators such as the beam power and the generalized beam power as a function of array geometry and signal to noise ratio. Optimal local-array geometries are suggested that are relevant to the problem of designing an optimal infrasound array.

Wave-number estimators along with estimated variance covariance matrices are used as input to study the size and orientation of 90% posterior probability ellipses for various likely subsets of detecting stations within the global infrasound array proposed for the Prototype International Data Center (IMS). Adding detecting stations decreased the size of the 90% ellipse by about 10-20% per added station, whereas increasing the signal to noise ratio from 2 to 3 decreased the size of the ellipse by 30-40%. Adding an inner triangle to the conventional 1 km triangular array gave more modest reductions of 7-10%.

Since the above conclusions are tentative and only apply to limited array configurations, any recommendations based on them should be considered as preliminary. The solution for a fixed configuration of recording arrays is not the only factor of interest since there will be multiple possible recording configurations possible for any given event. That is, the capability of the network will be an expected value, accumulated over possible recording configurations, weighted by the probability of each particular configuration. The resulting network capability can be contoured by setting an event at each location on the world-wide grid and then computing the probability that each station detects the event. We may then compute a weighted average of some parameter reflecting the location capability. For this discussion, we assume that the area of the 90% ellipse is of interest, where the ellipse may be a confidence ellipse under classical assumptions or a posterior probability ellipse under the Bayesian paradigm.

This might proceed in a manner that essentially parallels the *Networth* calculations made by Wirth et al (1976) in the case of seismic arrays. It would be most useful to develop an expression for the average area expected over all possible configurations of detecting arrays. That is, define a detection indicator D_k that is one if the array detects and is zero otherwise, for the full set of possible detecting arrays, say, for $k = 1, 2, \dots, K$ of them. If we define

$p_k = \text{Pr}\{D_k = 1\}$, the joint density of the random variables D_1, D_2, \dots, D_K would be

$$P(D_1, \dots, D_K) = \prod_{k=1}^K p_k^{D_k} (1 - p_k)^{1-D_k}. \quad (50)$$

The probabilities can be arbitrary for each station, based on recorded data or on the estimated probabilities computed from the result (4). Now, for any given event, we can observe 2^K possible configurations of detecting stations and each one of them will give a predicted area. We can multiply each configuration probability by its area and add them up to get the average areas of location for that particular source. Alternately, and perhaps, easier would be to simulate values of D_1, \dots, D_K repeatedly and simply average the resulting areas. In either case, it is clear that a relatively small computing effort will yield an average predicted 90% uncertainty area for each location. Plotting plotting the results as a grid of location contours on the map would give a more detailed index of potential global network performance.

Section 5

References

- Anderson, T.W. (1984). *An Introduction to Multivariate Statistical Analysis*. New York: Wiley.
- Blandford, R.R. (1996). Design of infrasonic arrays. *AFTAC Report AF-TR-97-013*, Headquarters, Air Force Technical Applications Center, Patrick AFB FL 32925-3002.
- Bratt, S.R. and T.C. Bache (1988). Locating events with a sparse network of regional arrays. *Bull. Seismolog. Soc. Amer*, 78, 780-798.
- Dempster, A.P., N.M. Laird and D.B. Rubin (1977). Maximum likelihood from incomplete data via the EM algorithm. *J. Royal Statist. Soc., B*, 39, 1-38.
- Evernden, J.F. (1969). Precision of epicenters obtained by small numbers of world-wide stations. *Bull Seismolog. Soc. Amer.*, 59, 1365-1398.
- Flinn, E.A. (1965). Confidence regions and error determinations for seismic event location. *Rev. Geophys.*, 3, 157-185.
- Jordan, T.H. and K.A. Sverdrup (1981). Teleseismic location techniques and their application to earthquake clusters in the South-Central Pacific, *Bull Seismolog. Soc. Amer*, 71, 1105-1130.
- Mack, H. and E.A. Flinn (1971). Analysis of the spatial coherence of short period acoustic gravity waves in the atmosphere. *Geophys. J.R. Astr. Soc.*, 26, 255-269.
- Meng, X.L. and D.B. Rubin (1993). Maximum likelihood estimation via the ECM algorithm: A general framework. *Biometrika*, 80, 267-278.
- Shumway, R.H., S.E. Kim and R.R. Blandford (1999). Nonlinear estimation for time series observed on arrays. Chapter 7, Ghosh ed. *Asymptotics, Nonparametrics and Time Series*, 227-258. New York: Marcel Dekker.
- Wirth, M.H. R.R. Blandford and R.H. Shumway(1976). Automatic seismic array and network detection. *Bull. Seismolog. Soc. Amer.*, 66, 1375-1380.

DISTRIBUTION LIST

DEPARTMENT OF DEFENSE

DIRECTOR
DEFENSE RESEARCH & ENGINEERING
WASHINGTON, DC 20301-3110
ATTN: DDR&E

DEFENSE TECHNICAL INFORMATION CENTER
8725 JOHN J. KINGMAN ROAD, SUITE 0944
FORT BELVOIR, VA 22060-6218
ATTN: DTIC/OCF

DEFENSE THREAT REDUCTION AGENCY
45045 AVIATION DRIVE
DULLES, VA 20166-7517
ATTN: TDCN, DR A. DAINTY
ATTN: TDS, DR C. GALLAWAY

DEFENSE THREAT REDUCTION AGENCY
6801 TELEGRAPH ROAD
ALEXANDRIA, VA 22310-3398
ATTN: CTR, L. KLUCHKO
ATTN: TD, DR D. LINGER
ATTN: TDANP, TRC
ATTN: TDC, M. SHORE
ATTN: TDCN, R. JIH

HEADQUARTERS
DEFENSE THREAT REDUCTION AGENCY
8725 JOHN J. KINGMAN ROAD, MS-6201
FT BELVOIR, VA 22060-6201
ATTN: TDCS, DR J. FOX

DEFENSE THREAT REDUCTION AGENCY
ALBUQUERQUE OPERATIONS
1680 TEXAS STREET, SE
KIRTLAND AFB, NM 87117-5669
ATTN: TDT-D, DR G. BALADI
ATTN: TDTP, DR B. RISTVET

DEPARTMENT OF DEFENSE CONTRACTORS

ACIS
6T11 NHB
WASHINGTON, DC 20505
ATTN: DR J. FILSON
ATTN: L. TURNBULL
ATTN: T. MURPHY

BATTELLE MEMORIAL INSTITUTE
MUNITIONS & ORDNANCE CTR
505 KING AVENUE
COLUMBUS, OH 43201-2693
ATTN: TACTEC

BBN CORPORATION
1300 N. 17TH STREET, SUITE 1200
ARLINGTON, VA 22209
ATTN: H. FARRELL
ATTN: J. PULLI

BDM CORPORATION OF SAUDI ARABIA
12150 EAST MONUMENT DRIVE, SUITE 501
FAIRFAX, VA 22033-4050
ATTN: J. STOCKTON, JB 4C22

CALIFORNIA, UNIVERSITY AT SAN DIEGO
SCRIPPS INSTITUTION OF OCEANOGRAPHY
P. O. BOX 6049
SAN DIEGO, CA 92166-6049
ATTN: C. DEGROOT-HEDLIN
ATTN: DR M. A. H. HEDLIN
ATTN: PROF F. VERNON
ATTN: PROF J. A. ORCUTT
ATTN: PROF J. BERGER

CENTER FOR MONITORING RESEARCH
1300 N. 17TH STREET, SUITE 1450
ARLINGTON, VA 22209
ATTN: DR K. L. MCLAUGHLIN
ATTN: DR R. NORTH
ATTN: LIBRARIAN
ATTN: R. A. GUSTAFSON
ATTN: V. RYABOY

CTB TREATY MANAGER
ROSSLYN GATEWAY
1901 N. MOORE STREET, SUITE 609
ARLINGTON, VA 22209
ATTN: DR R. W. ALEWINE, III

DGI
3612 SURFWOOD RD
MALIBU, CA 90265
ATTN: R. F. HERBST

ENSCO, INC
445 PINEDA COURT
MELBOURNE, FL 3940
ATTN: DR D. TAYLOR

ENSCO, INC.
P. O. BOX 1346
SPRINGFIELD, VA 22151-0346
ATTN: D. BAUMGARDT
ATTN: Z. DER

DEPARTMENT OF DEFENSE CONTRACTORS

GEOPEX, LTD.
WESTON GEOPHYSICAL
325 WEST MAIN STREET
NORTHBOROUGH, MA 01532
ATTN: DR D. REITER
ATTN: MR J. LEWKOWICZ

ITT INDUSTRIES
ITT SYSTEMS CORPORATION
ATTN: AODTRA/DTRIAC
1680 TEXAS STREET, SE
KIRTLAND AFB, NM 87117-5669
ATTN: DTRIAC
ATTN: DTRIAC/DARE

JAYCOR
1410 SPRING HILL ROAD, SUITE 300
MCLEAN, VA 22102
ATTN: DR C. P. KNOWLES
ATTN: T. J. HANNIGAN

JAYCOR, INC.
P. O. BOX 85154
SAN DIEGO, CA 92138-5154
ATTN: M. TREADAWAY
ATTN: R. STAHL

LACHEL & ASSOCIATES INC.
P. O. BOX 5266
GOLDEN CO 80401
ATTN: D. LACHEL

LOGICON INC.
LOGICON ADVANCED TECHNOLOGY
2100 WASHINGTON BLVD
ARLINGTON, VA 22204-5704
ATTN: F. DICKERSON

LOGICON R AND D ASSOCIATES
P. O. BOX 100
PAHRUMP, NV 89041
ATTN: J. LACOMB

MAXWELL LABORATORIES, INC.
S-CUBED WASHINGTON RESEARCH OFFICE
11800 SUNRISE VALLEY DRIVE, SUITE 1212
RESTON, VA 22091
ATTN: DR. T. J. BENNETT
ATTN: J. R. MURPHY

MAXWELL TECHNOLOGIES INC.
SYSTEMS DIVISION
9210 SKY PARK COURT
SAN DIEGO, CA 92123-4302
ATTN: DR E. PETERSON
ATTN: DR J. L. STEVENS
ATTN: DR G. E. BAKER

MISSION RESEARCH CORP.
8560 CINDERBED ROAD, SUITE 700
NEWINGTON, VA 22122
ATTN: DR. M. FISK

MULTIMAX, INC
1441 MC CORMICK DRIVE
LANDOVER, MD 20785
ATTN: DR I. N. GUPTA
ATTN: DR W. CHAN
ATTN: MS L. GRANT

PACIFIC NORTHWEST LABORATORIES
A DIV OF BATTELLE MEMORIAL INST.
P. O. BOX 999
RICHLAND, MA 99352
ATTN: TECHNICAL STAFF, MS K5-12

PACIFIC-SIERRA RESEARCH CORP.
WASHINGTON OPERATIONS
1400 KEY BOULEVARD, SUITE 700
ARLINGTON, VA 22209
ATTN: N. L. DUNCAN

S-CUBED
A DIVISION OF MAXWELL LABS, INC.
11800 SUNRISE VALLEY DRIVE, SUITE 1212
RESTON, VA 22091
ATTN: J. MURPHY

SCIENCE & ENGINEERING ASSOCIATES, INC.
7918 JONES BRANCH DRIVE, SUITE 500
MCLEAN, VA 22102
ATTN: R. BEATY

SCIENCE APPLICATION INT'L CORP.
3309 NW GOLDEN PLACE
SEATTLE, WA 98117
ATTN: A. RATLETON

SCIENCE APPLICATIONS INTL CORP.
10260 CAMPUS POINT DRIVE
SAN DIEGO, CA 92121-1578
ATTN: DR T. C. BACHE, JR.
ATTN: DR T. J. SERENO, JR.

SCIENCE APPLICATIONS INTL CORP
2111 EISENHOWER AVENUE, SUITE 205
ALEXANDRIA, VA 22314
ATTN: DR D. PIEPENBURG

SCIENCE APPLICATIONS INTL CORP.
GEOSPATIAL DATA DEVELOPMENT DIVISION
700 SOUTH BABCOCK STREET, SUITE 300
MELBOURNE, FL 32901
ATTN: R. BJURSTROM

SCIENCE APPLICATIONS INTL CORP.
P. O. BOX 1303
MCLEAN, VA 22102
ATTN: D. BACON

SOUTHERN METHODIST UNIVERSITY
DEPT OF GEOLOGICAL SCIENCE
P. O. BOX 395
DALLAS, TX 75275-0395
ATTN: DR B. STUMP
ATTN: E. HERRIN

SRI INTERNATIONAL
333 RAVENSWOOD AVENUE
MENLO PARK, CA 94025-3434
ATTN: D. CURRAN

ST LOUIS UNIVERSITY
P. O. BOX 8148
PIERRE LACLEDE STATION
ST LOUIS, MO 63156-8148
ATTN: PROF B. HERRMANN
ATTN: PROF B. J. MITCHELL

TASC, INC
1101 WILSON BOULEVARD, SUITE 1500
ARLINGTON, VA 22209-2248
ATTN: J. A. MOSORA

TEXAS, UNIVERSITY AT AUSTIN
P. O. BOX 7726
AUSTIN, TX 78712
ATTN: C. A. FROELICH

WOODWARD-CLYDE CONSULTANTS
566 EL DORADO STREET
PASADENA, CA 91109-3245
ATTN: DR B. B. WOODS
ATTN: DR C. K. SAIKIA

DEPARTMENT OF ENERGY

BECHTEL NEVADA
P. O. BOX 809
LOS ALAMOS, NM 87544-0809
ATTN: D. EILERS

BECHTEL NEVADA, INC
P. O. BOX 98521
LAS VEGAS, NV 89193-8521
ATTN: D. BARKER, M/S NLV053

DEPARTMENT OF ENERGY
1000 INDEPENDENCE AVENUE SW
WASHINGTON, DC 20585
ATTN: D. WATKINS, NN-42/GA007
ATTN: E. MANAK, NN-30/FORS
ATTN: E. STOVER
ATTN: S. RUDNICK/NN-20

UNIVERSITY OF CALIFORNIA
LAWRENCE LIVERMORE NATIONAL LAB
P. O. BOX 808
LIVERMORE, CA 94551-9900
ATTN: K. NAKANISHI
ATTN: W. J. HANNON, JR, MS, L-103
ATTN: F. HEUZE, MS, L-200
ATTN: L. GLENN, MS, L-200
ATTN: DR J. ZUCCA, MS, L-205
ATTN: M. DENNY, MS, L-205
ATTN: TECHNICAL STAFF, MS, L-200
ATTN: TECHNICAL STAFF, MS, L-208
ATTN: TECHNICAL STAFF, MS, L-205

LOS ALAMOS NATIONAL LABORATORY
P. O. BOX 1663
MAIL STOP G-733
LOS ALAMOS, NM 87545
ATTN: F. CHAVEZ, MS-D460
ATTN: D. WESTERVELT, MS-A112
ATTN: D. STEEDMAN, MS-F607
ATTN: TECHNICAL STAFF, MS-C335
ATTN: TECHNICAL STAFF, MS-D460
ATTN: TECHNICAL STAFF, MS-F665

PACIFIC NORTHWEST NATIONAL
LABORATORY
P. O. BOX 999
BATTELLE BOULEVARD
RICHLAND, WA 99352
ATTN: D. N. HAGEDORN, MS K5-12

SANDIA NATIONAL LABORATORIES
ATTN: MAIL SERVICES
P. O. BOX 5800
ALBUQUERQUE, NM 87185-0459
ATTN: TECHNICAL STAFF, DEPT 5704,
MS 0655
ATTN: TECHNICAL STAFF, DEPT 5704,
MS 0979
ATTN: TECHNICAL STAFF, DEPT 5736,
MS 0655
ATTN: TECHNICAL STAFF, DEPT 9311,
MS 1159

SEISMOLOGICAL LABORATORY 252-21
CALIFORNIA INSTITUTE OF TECHNOLOGY
PASADENA, CA 91125
ATTN: T. AHERNS

UNIVERSITY OF CALIFORNIA
EARTH SCIENCE DIVISION
479 MCCONE HALL, LBNL, 90-2108
BERKELEY, CA 94720
ATTN: L. JOHNSON, MS-90-1116

DEPARTMENT OF THE AIR FORCE

HEADQUARTERS
AFTAC/TTR
1030 SOUTH HIGHWAY A1A
PATRICK AFB, FL 32925-3002
ATTN: V. HSU

AIR FORCE RESEARCH LABATORY
29 RANDOLPH ROAD
HANSCOM AFB, MA 01731-5000
ATTN: DR D. HARKRIDER
ATTN: DR D. REITER
ATTN: GPE, J. LEWKOWICZ
ATTN: J. RONG-SONG

AIR FORCE RESEARCH LABORATORY
5 WRIGHT STREET
HANSCOM AFB, MA 01731-3004
ATTN: RESEARCH LIBRARY, TL

AIR FORCE TECH APPLICATIONS CENTER
1300 17TH STREET, SUITE 1450
ARLINGTON, VA 22209
ATTN: R. BLANDFORD

AIR FORCE TECHNICAL APPLICATIONS
CTR/TT
1030 S HIGHWAY A1A
PATRICK AFB, FL 32925-3002
ATTN: CA/STINFO
ATTN: DR B. KEMERAIT
ATTN: DR D. RUSSELL
ATTN: G. ROTHE, TTR
ATTN: J. C. LUCAS
ATTN: M. SIBOL

**DIRECTORY OF OTHER (LIBRARIES AND
UNIVERSITIES)**

ARIZONA, UNIVERSITY OF
DEPT. OF GEOSCIENCES/SASO
TUCSON, AZ 85721
ATTN: PROF T. C. WALLACE

BOISE STATE UNIVERSITY
GEOSCIENCES DEPARTMENT
1910 UNIVERSITY DRIVE
BOISE, ID 83725
ATTN: J. E. ZOLLWEG

BOSTON COLLEGE
INSTITUTE FOR SPACE RESEARCH
140 COMMONWEALTH AVENUE
CHESTNUT HILL, MA 02167
ATTN: PROF L. SYKES

CALIFORNIA INSTITUTE OF TECHNOLOGY
DIVISION OF GEOLOGY & PLANETARY
SCIENCES
PASADENA, CA 91125
ATTN: PROF D. V. HELMBERGER

CALIFORNIA-DAVIS, UNIVERSITY OF
DAVIS, CA 95616
ATTN: R. H. SHUMWAY, DIV STATISTICS
ATTN: S. E. KIM

CALIFORNIA-SANTA CRUZ, UNIVERSITY OF
INSTITUTE OF TECTONICS
SANTA CRUZ, CA 95064
ATTN: DR R. S. WU
ATTN: PRO T. LAY

COLORADO-BOULDER, UNIVERSITY OF
BOULDER, CO 80309
ATTN: M. RITZWOLLER,
CAMPUS BOX 390
ATTN: PROF C. ARCHAMBEAU

COLUMBIA UNIVERSITY
LAMONT-DOHERTY EARTH OBSERVATORY
PALISADES, NY 10964
ATTN: DR L. R. SYKES
ATTN: DR J. XIE
ATTN: PROF P. G. RICHARDS

CONNECTICUT, UNIVERSITY OF
DEPT. OF GEOLOGY & GEOPHICS
STOORS, CT 06269-2045
ATTN: PROF V. F. CORMIER, U-45,
ROOM 207

CORNELL UNIVERSITY
DEPARTMENT OF GEOLOGICAL SCIENCES
3126 SNEE HALL
ITHACA, NY 14853
ATTN: PROF M. BARAZANGI

HARVARD UNIVERSITY
HOFFMAN LABORATORY
20 OXFORD STREET
CAMBRIDGE, MA 02138
ATTN: PROF A. DZIEWONSKI
ATTN: PROF G. EKSTROM

IRIS
1200 NEW YORK AVENUE, NW, SUITE 800
WASHINGTON, DC 20005
ATTN: DR D. SIMPSON
ATTN: DR G. E. VAN DER VINK

MASSACHUSETTS INSTITUTE
OF TECHNOLOGY
EARTH RESOURCES LABORATORY
42 CARLETON STREET
CAMBRIDGE, MA 02142
ATTN: PROF M. N. TOKSOZ

MICHIGAN STATE UNIVERSITY LIBRARY
450 ADMINISTRATION BUILDING
EAST LANSING, MI 48824
ATTN: K. FUJITA

NEW MEXICO STATE UNIVERSITY
DEPARTMENT OF PHYSICS
LAS CRUCES, NM 88003
ATTN: PROF J. NI
ATTN: PROF T. HEARN

PENNSYLVANIA STATE UNIVERSITY
GEOSCIENCES DEPARTMENT
403 DEIKE BUILDING
UNIVERSITY PARK, PA 16802
ATTN: PROF C. A. LANGSTON
ATTN: PROF S. ALEXANDER

SAN DIEGO STATE UNIVERSITY
DEPT OF GEOLOGICAL SCIENCES
SAN DIEGO, CA 92182
ATTN: PROF S. M. DAY

SOUTHERN METHODIST UNIVERSITY
FONDREN LIBRARY
DALLAS, TX 75275
ATTN: B. STUMP
ATTN: G. MCCARTOR, DEPT OF PHYSICS
ATTN: H. L. GRAY, DEPT OF STATISTICS

UNIVERSITY OF COLORADO
CAMPUS BOX 583
BOULDER, CO 80309
ATTN: DR A. L. LEVSHIN

UNIVERSITY OF SOUTHERN CALIFORNIA
520 SEAVER SCIENCE CENTER
UNIVERSITY PARK
LOS ANGELES, CA 90089-0483
ATTN: PROF C. G. SAMMIS

FOREIGN

AUSTRALIAN GEOLOGICAL
SURVEY ORGANIZATION
CORNER OF JERRAGOMRRRA AND
NINDMARSH DRIVE
CANBERRA, ACT 2609
AUSTRALIA
ATTN: D. JEPSON

GEOPHYSICAL INSTITUTE OF ISRAEL
HAMASHBIR STREET, 1
HOLON, 58122 ISRAEL
ATTN: DR Y. GITTERMAN

I.R.I.G.M. - B.P. 68
38402 ST. MARTIN D'HERES
CEDEX, FRANCE
ATTN: DR M. BOUCHON

MINISTRY OF DEFENSE/
PROCUREMENT EXECUTIVE
ALACKNESS, BRIMPTON
READING FG7-4RS ENGLAND
ATTN: DR P. MARSHALL

NTNF/NORSAR
P. O. BOX 51
N-2007 KJELLER, NORWAY
ATTN: DR F. RINGDAL
ATTN: T. KVAERNA

OBSERVATOIRE DE GRENOBLE
I.R.I.G.M. - B.P. 53
38041 GRENOBLE, FRANCE
ATTN: DR M. CAMPILLO

RESEARCH SCHOOL OF EARTH SCIENCES
INSTITUTE OF ADVANCES STUDIES
G. P. O. BOX 4
CANABERRA 2601, AUSTRALIA
ATTN: PROF B. L. N. KENNETT

RUHR UNIVERSITY/BOCHUM
INSTITUTE FOR GEOPHYSIK
P. O. BOX 102148
463 BOCHUM 1, GERMANY
ATTN: PROF H. P. HARJES

SEISMOLOGICAL DIVISION
IRPG
P.O. BOX 2286
HOLON 58122
ISRAEL

ATTN: A. SHAPIRA

SOCIETE RADIOMANA
27 RU CLAUDE BERNARD
75005 PARIS, FRANCE
ATTN: DR B. MASSINON
ATTN: DR P. MECHLER

UNIVERSITY OF BERGEN
INSTITUTE FOR SOLID EARTH PHYSICS
ALLEGATION 40
N-5007 BERGEN, NORWAY
ATTN: R. E. HUSEBYE

UNIVERSITY OF CAMBRIDGE
DEPARTMENT OF EARTH SCIENCES
MADINGLEY RISE, MADINGLEY ROAD
CAMBRIDGE CB3 0EZ, ENGLAND
ATTN: PROF K. PRIESTLEY

OTHER GOVERNMENT

CENTRAL INTELLIGENCE AGENCY
WASHINGTON, DC 20505
ATTN: CHIEF, OTI/MNG/NWTT - ST47 NHB

NATIONAL ARCHIVES AND
RECORDS ADMINISTRATION
8601 ADELPHI ROAD, ROOM 3360
COLLEGE PARK, MD 20740-6001
ATTN: USER SERVICE BRANCH

NATIONAL PHOTOGRAPHIC
INTERPRETATION CENTER
SOUTHWEST STATION
P. O. BOX 70967
WASHINGTON, D C 20024-0967
ATTN: K. TIGHE-WHITE
ATTN: M. BURNS

U S DEPARTMENT OF STATE
320 21ST STREET, NW
WASHINGTON, DC 20451
ATTN: DR E. LACEY, ACDA/VI,
ROOM 5741
ATTN: K. WARD
ATTN: R. DAY
ATTN: T. RAY

US DEPARTMENT OF THE INTERIOR
US GEOLOGICAL SURVEY NATIONAL CENTER
MILITARY GEOLOGY PROJECT
12201 SUNRISE VALLEY DRIVE
RESTON, VA 22029
ATTN: B. LEITH
ATTN: DR J. FILSON
ATTN: W. LEITH, MS 928

DISTRIBUTION LIST UPDATE

This mailer is provided to enable DTRA to maintain current distribution lists for reports. (We would appreciate you providing the requested information.)

- ☐ Add the individual listed to your distribution list.
- ☐ Delete the cited organization/individual.
- ☐ Change of address.

Note:

Please return the mailing label from the document so that any additions, changes, corrections or deletions can be made easily. For distribution cancellation or more information call DTRA/ADM (703) 767-4724.

NAME: _____

ORGANIZATION: _____

OLD ADDRESS

NEW ADDRESS

TELEPHONE NUMBER: () _____

DTRA PUBLICATION NUMBER/TITLE

CHANGES/DELETIONS/ADDITIONS, etc.)

(Attach Sheet if more Space is Required)

DTRA or other GOVERNMENT CONTRACT NUMBER: _____

CERTIFICATION of NEED-TO-KNOW BY GOVERNMENT SPONSOR (if other than DTRA):

SPONSORING ORGANIZATION: _____

CONTRACTING OFFICER or REPRESENTATIVE: _____

SIGNATURE: _____

CUT HERE AND RETURN

DEFENSE THREAT REDUCTION AGENCY
ATTN: ADM
8725 John J. Kingman Road, MS-6201
Ft Belvoir, VA 22060-6201

DEFENSE THREAT REDUCTION AGENCY
ATTN: ADM
8725 John J. Kingman Road, MS-6201
Ft Belvoir, VA 22060-6201